Computational Materials Science 47 (2010) 752–757

Contents lists available at ScienceDirect

Computational Materials Science

journal homepage: www.elsevier.com/locate/commatsci

Bond analysis of phosphorus skutterudites: Elongated lanthanum electron buildup in $LaFe_4P_{12}$

Espen Flage-Larsen *, Ole Martin Løvvik, Øystein Prytz, Johan Taftø

Department of Physics, University of Oslo, PO Box 1048, Blindern, NO-0316 Oslo, Norway

ARTICLE INFO

Article history:
Received 26 June 2009
Received in revised form 28 October 2009
Accepted 29 October 2009

PACS:
61.50.Lt
63.20.−e
71.15.Mb
71.20.Eh
71.20.Be
72.10.Di
72.15.Jf

Keywords:
Skutterudite
Thermoelectric materials
Electronic properties

ABSTRACT

Electron transfer and bonding characteristics of a selected set of phosphorus skutterudites are investigated using density functional calculations. Electron transfer for CoP_3, $LaFe_4P_{12}$ and the hypothetical FeP_3 compounds are calculated using procrystals as the non-binding references. Spherical integration and Bader analysis are performed to quantify electron transfer differences between these compounds. The results are in good qualitative agreement with simple electronegativity considerations. The calculations confirm that the transition metal–phosphorus and the phosphorus–phosphorus bonds are covalent, while the lanthanum–phosphorus bond is of a more polar and complex nature. In addition, we describe a unique bonding scheme between lanthanum and phosphorus where elongated electron buildup along the crystal axes surround the lanthanum ion. This is identified as a likely reason for the special phonon-scattering properties of the lanthanum filler ion.

1. Introduction

In recent years, skutterudite compounds have attracted much attention as potential thermoelectric materials [1]. This is mainly attributed to their high figure-of-merit [1] and the possibility to substitute and modify the composition while still retaining the basic structure [2]. The efficiency of a thermoelectric material is determined by the figure-of-merit is defined as $ZT = \alpha^2\sigma T/\kappa$, where α, σ, κ and T are the Seebeck coefficient, the electrical conductivity, the thermal conductivity, and the temperature, respectively. The high ZT value comes as a result of a strong asymmetric density of states near the Fermi energy and the ability to drastically decrease the thermal conductivity by adding interstitial atoms. These structures are also interesting due to superconducting [3,4], heavy-fermion [5,6] and ferromagnetic [7] behaviour.

Empty skutterudite compounds in space group $Im\bar{3}$ have the chemical formula MX_3, where M and X are transition metals and pnictogens (elements in the nitrogen group), respectively. The completely filled RM_4X_{12} skutterudite structure is illustrated in Figs. 1 and 2. Usually, R is a rare-earth metal.

It was early suggested [8] that filling the open voids could reduce the thermal conductivity. This idea has since been confirmed [9] and also discovered in other similar compounds. The decrease of the thermal conductivity is attributed to the filler atoms, which has been detected in inelastic neutron diffraction studies [10]. Changes of the thermal conductivity have also been shown for substitutions in the basic skutterudite framework [11–13].

The true nature of the lower thermal conductivity has been discussed in the literature. It is commonly believed that the filler ions can "rattle" independently [14] in the dodecahedra of X ions. However, recent studies [15,16] used neutron spectroscopy combined with ab-initio calculations to show a more correlated motion of the filler ions. These studies also argue that the phonon dampening is caused by a significant flattening of the phonon bands.

Previous investigations [17] shed light on the importance of the hybridization between the p- and d-orbitals of the pnictogens and transition metals to stabilize the $CoSb_3$ compound. The lowest conduction band responsible for electron transport was shown to include mainly Sb p-states located in the Sb_4 ring [17]. These rings were furthermore shown to be connected through the $CoSb_6$ octahedra by the highest valence band. In addition, evidence of delocalized non-bonding Sb s-states was observed.

* Corresponding author.
E-mail address: espen.flage-larsen@fys.uio.no (E. Flage-Larsen).

0927-0256/$ - see front matter © 2009 Elsevier B.V. All rights reserved.
doi:10.1016/j.commatsci.2009.10.018

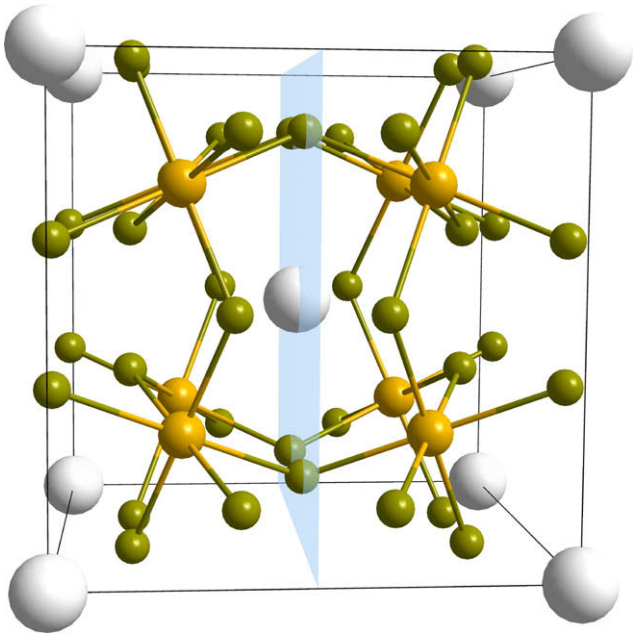

Fig. 1. The filled skutterudite structure. Small, medium and large spheres are the pnictogens, transition metals and filler ions, respectively. The octahedral arrangement of pnictogens around the transition metal and the (200) plane are shown.

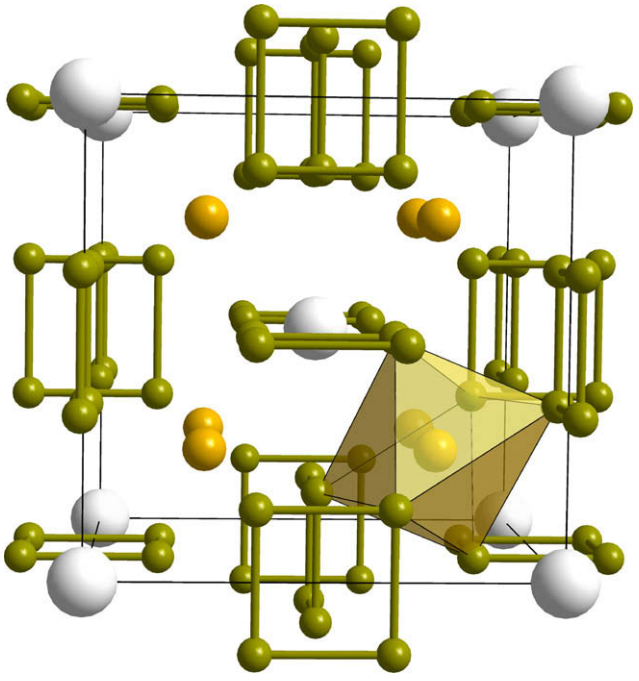

Fig. 2. The filled skutterudite structure. Small, medium and large spheres are the pnictogens, transition metals and filler ions, respectively. The octahedral arrangement of pnictogens around the transition metal and pnictogen rings are shown.

There have been discussions [18] as to whether it is the MX_6 octahedra, the X_4 ring or a combination of both [17] that determine the main bonding features of the skutterudite compounds. Previous studies [19,20] have calculated and measured the density of states around the Fermi level. From these studies it is quite clear that the 3d-states of M lie right under the Fermi level followed by the 3p-states of X, while the X 3s-states lie deep below the Fermi level and are not significantly contributing to bonding. The lower part of the conduction band has primarily 3d- and 3p-state character from M and X respectively [19,20].

To our knowledge the bonding character of the filler ions has not been specifically addressed in detail beyond what has been suggested in literature reviews [9,21], in spite of the their special role in enhancing the lattice thermal resistivity. The recent studies [15,16] suggesting a correlated movement of the filler atoms motivated us to specifically address the filler ion electron transfers.

Bond analysis is often done in a state-resolved formalism by means of the electron band structure and density of states. Even though the state-resolved approach can give significant insight in the bonding scheme, it does not provide direct spatial information. Furthermore, it may be difficult to assign a direct quantitative experimental verification in this scheme. Another option is to use a space-resolved analysis. In this case there is a direct relation between the electron density and the structure factors. Precise X-ray or electron diffraction can thus provide a reliable, quantitative reference for the calculations. To compliment previous state-resolved studies [19,20] we investigate in this study the bonding and electron transfer of phosphorus skutterudites in a space-resolved formalism.

2. Computational details

2.1. Electron transfer analysis

The electron transfer ρ_b in a material can be defined by

$$\rho_b = \rho_0 - \rho_r, \tag{1}$$

where ρ_r is a reference electron charge density and ρ_0 is the crystal electron charge density of the material. Bonding properties can then be quantified and visualized from ρ_b. In this work we use the procrystal [22] ρ_p electron density as the reference. The electron density of the procrystal contains non-bonding, but overlapping atomic electron densities.

Assigning quantitative electrons to an ion is difficult, and a number of different approaches are being used [23]. In this work we will use a Bader analysis [24] scheme to determine the quantitative ionic electron occupancy numbers. The underlying principle of the Bader analysis is a electron charge partitioning based on zero flux surfaces in the electron density. The implementation of the Bader analysis used in this work [25–28] relies on a core representation of the electron density to be included as a reference. This is a potential problem due to the rapid fluctuation near the core. However, calculations of the occupancies are done purely on the valence density grid. Due to finite grid resolution the Bader analysis can return different values for symmetry equivalent positions (1% difference in the occupancies is observed for the P ions). In those cases, the average occupancies are given.

An alternative way to determine quantitative electron transfer is to perform spherical integration around the ions. This raises three fundamental objections. In general the bonds are not spherically symmetric, and the unit cell volume cannot be covered by spheres alone, which means that parts of the electron density must escape the analysis. Finally, the freedom to choose sphere radii complicates comparison studies. Nevertheless, a spherical body shape is simple to define and intuitively easy to analyse. In this work we have therefore used spherical integration to calculate the electron depletion around each ion, well aware of its limitations.

A common approach is to use the covalent radius as a cutoff during the spherical integration. This is obviously a simplification and may be unreasonable for bonds not obeying covalency. In this work we suggest an alternative way to set the radial cutoff r_d to give a quantitative measure of the electron depletion. We start

by integrating the electron density difference ρ_b from which information about the electron transfer is directly available. We define the integral I_b as

$$I_b(r) = \int_{-r}^{r} \int_{y_1}^{y_2} \int_{z_1}^{z_2} \rho_b(x,y,z) dz dy dx, \quad (2)$$

where $z_1 = -\sqrt{r^2 - x^2 - y^2}, z_2 = -z_1, y_1 = -\sqrt{r^2 - x^2}$ and $y_2 = -y_1$. The volume of integration is thus limited by the outer cutoff radius r. The electron depletion number Δn_d is defined as

$$\Delta n_d = I_b(r = r_d). \quad (3)$$

In this work r_d is defined as the radius where the integral I_b peaks. More specifically as

$$\left.\frac{dI_b(r)}{dr}\right|_{r=r_d} = 0. \quad (4)$$

We require that $r_d > r_t$, a lower threshold limit. Choosing this threshold limit can be difficult in general and will depend on the approach used to generate the electron density. For the compounds in this work we found that a value of $r_t = 0.3$ Å avoids possible local extrema close to the core. Controllable accuracy during the integration has been obtained by the use of a numerical trapezoidal integration scheme. This relies on the modified Shepard interpolation routine [29] which allows a correct representation close to the integration limits without severe performance penalties.

Furthermore, we have calculated the mean value of the depletion $\langle \Delta n_d \rangle$ by integrating I_b such that

$$\langle \Delta n_d \rangle = \frac{1}{r_d} \int_0^{r_d} I_b(r) dr. \quad (5)$$

Typically a small difference between $\langle \Delta n_d \rangle$ and Δn_d indicates an abrupt and short-ranged depletion around the ion, while a more spread out depletion is true for a larger difference. This and the value of r_d give information about the extension of the depletion. A limitation of this method is that occupancy numbers can not be obtained.

To compare electron transfer maxima locations and their covalent character we have defined the centre of Pauling electronegativity as $\chi^* = \chi_1/(\chi_1 + \chi_2)$, where χ_1 and χ_2 are the Pauling electronegativities of the respective ions.

2.2. Density functional theory

The electron densities were obtained by performing density functional theory (DFT) [30,31] calculations in the PBE generalized gradient approximation [36] exchange correlation functional. The highly efficient projector-augmented-wave (PAW) [37,38] method was also used. All calculations were done using the Vienna *Ab-initio* Simulation Package (VASP) [38–43].

Crystal structures were relaxed in cell size, shape and atomic positions using the residual minimization scheme, direct inversion in the iterative subspace (RMM–DIIS) [44] algorithm. After the relaxation another self-consistent calculation was done to ensure correct representation of the system. An energy cutoff of 800 eV and 550 eV for $LaFe_4P_{12}$ and CoP_3 were necessary to obtain convergence of the total energy to within 2 meV. A k-point grid of $8 \times 8 \times 8$ for the conventional (cubic) unit cell was sufficient to achieve similar convergence. The finer FFT grid where the augmentation charge is evaluated was sized three times that of the normal FFT grid. The $5s^2 5p^6 5d^1 6s^2$, $3d^7 4s^2$, $3d^6 4s^2$ and $3s^2 3p^3$ electrons were treated as valence orbitals for La, Co, Fe and P, respectively.

Comparable smearing conditions are important during this type of electron charge analysis, since different smearing parameters will affect the results well above errors introduced in the post-processing. A Gaussian smearing [45] of 0.3 eV was needed to converge the total energies of all structures to within 1 μeV. The difference between Gaussian and higher order Methfessel and Paxton smearing [46] was found to be very small for $LaFe_4P_{12}$, thus Gaussian smearing was used in all cases. Procrystal electron densities were generated from free atomic electron densities obtained from single atom calculations using VASP. For the single atom calculations, a $2 \times 2 \times 2$ unit cell was used to avoid any bonding with neighbouring cells. To make sure that the resolution was comparable for the augmentation charges, the grid size was adjusted accordingly.

The need for a correct representation of the all-electron charge density must be emphasized. Due to the compensator charge density [38] the usual charge density obtained from VASP is not the true all-electron charge density. In this work the all-electron density has been explicitly regenerated after a pre-converged run, thus removing the problems associated with the compensator electron density. For the Bader analysis the total electron density (valence and core) has been included as a reference to ensure proper determination of extremal points in the electron density. For all other calculations in this work the separated all-electron valence density has been used exclusively.

3. Results and discussion

3.1. Structural relaxation

Experimental lattice parameters and atomic positions were used as starting points for the structural relaxation of CoP_3 and $LaFe_4P_{12}$. Results are shown in Table 1. Lattice constants and Wyckoff positions of all relaxed structures were within one percent of the experimental values and previous calculated results [47–49,20]. For the hypothetical FeP_3 we used crystal parameters of CoP_3. In agreement with earlier reports [47–49], the P_4 ring becomes more square going from CoP_3 to $LaFe_4P_{12}$, where the P_4 width to length ratio is 0.79 and 0.97, respectively.

3.2. Electron transfer analysis around the transition metal and pnictogen atoms

This discussion will rely on the comparison of inter-ionic line extraction data of ρ_b for CoP_3, FeP_3 and $LaFe_4P_{12}$ in Figs. 3 and 4. To ease the comparison, data from the line extractions are summarized in Table 4. Depletion numbers and Bader analysis data are presented in Tables 2 and 3. Due to the finite grid resolution and centring issues we have excluded the region close to the ions for the inter-ionic line extractions (less than 0.2 Å from the core center for all compounds).

The electron depletion Δn_d from Table 2 is largest around La and Co, followed by Fe and then P. In general these numbers follow what is expected from the electronegativities. Comparing the average depletion number $\langle \Delta n_d \rangle$ and depletion cutoff r_d around each ion yields evidence of a depletion zone around La that extends further out than around Fe, Co and P. Even though this is natural to expect from the size of La, there is still significantly smaller difference between the depletion cutoff and the covalent radius compared to the other ions. It is also important to note that the

Table 1
The lattice constant a, and position parameters y and z for the relaxed CoP_3 and $LaFe_4P_{12}$ structure.

	a [Å]	y	z
CoP_3	7.722	0.348	0.146
$LaFe_4P_{12}$	7.827	0.353	0.152

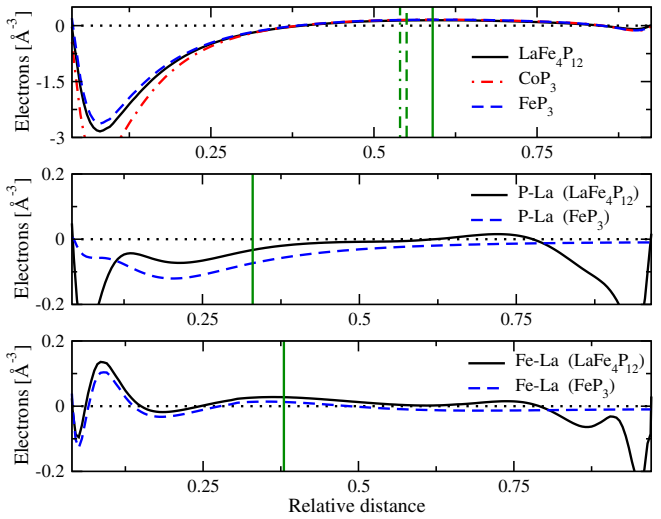

Fig. 3. Inter-ionic extraction of the electron density difference ρ_b along the *M*-P (upper), P–La (middle) and Fe–La (lower) line. The transition metals Co and Fe are designated *M*. In the upper plot a comparison between $LaFe_4P_{12}$ (solid line), CoP_3 (dashed-dotted line) and FeP_3 (dashed line) is given, while in the middle a comparison of ρ_b along P–La in $LaFe_4P_{12}$ (solid line) and FeP_3 (dashed line) is given. The lower plot shows the same comparison as the middle plot, except now for ρ_b along Fe–"La". "La" represents Wyckoff position *a* where e.g. La atoms would have been located. The distances are normalized and features close to the ion centres have been excluded. Center of Pauling electronegativities from Table 4 are shown in green. (For interpretation of the references to colour in this figure legend, the reader is referred to the web version of this article.)

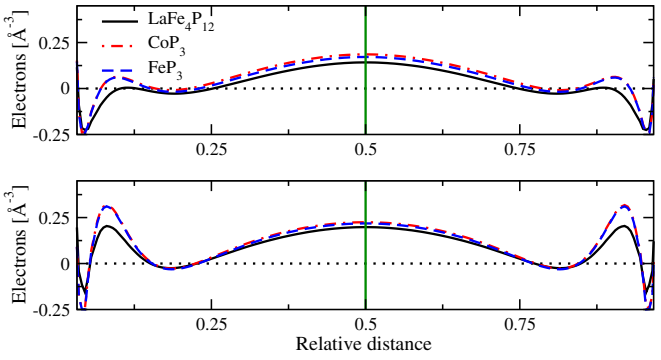

Fig. 4. Inter-ionic extraction of the electron density difference ρ_b between the long P–P bonds (upper) and its shorter counterpart (lower). A comparison between $LaFe_4P_{12}$ (solid line), CoP_3 (dashed-dotted line) and FeP_3 (dashed line) is given. The distances are normalized and features close to the ions centres have been excluded. Center of Pauling electronegativities from Table 4 are shown in green. (For interpretation of the references to colour in this figure legend, the reader is referred to the web version of this article.)

Table 2
Spherical depletion numbers Δn_d and their mean values $\langle \Delta n_d \rangle$, the cutoff radii r_d and the Pauling electronegativities [50,51] χ are shown. The covalent radii r_c [52] are also listed for comparison.

	Δn_d	$\langle \Delta n_d \rangle$	r_d [Å]	r_c [Å]	χ
CoP_3					
Co	−0.24	−0.01	0.80	1.26	1.88
P	−0.05	−0.02	0.80	1.07	2.19
FeP_3					
Fe	−0.22	−0.09	0.84	1.32	1.83
P	−0.05	−0.02	0.80	1.07	2.19
$LaFe_4P_{12}$					
Fe	−0.22	−0.09	0.84	1.32	1.83
P	−0.06	−0.02	0.84	1.07	2.19
La	−0.24	−0.11	1.99	2.07	1.10

Table 3
Bader analysis of CoP_3, FeP_3 and $LaFe_4P_{12}$. Both the electronic occupancy number and the minimum distance to the Bader surface are given. The occupancy difference is relative to the formal valence occupancy of the free atom. For the P ions, the average values are given.

	Valence electrons			Minimal distance [Å]
	Atom	Crystal	Difference	
CoP_3				
Co	9.0	8.89	−0.11	1.02
P	5.0	5.04	0.04	1.12
FeP_3				
Fe	8.0	7.78	−0.22	1.00
P	5.0	5.08	0.08	1.11
$LaFe_4P_{12}$				
Fe	8.0	7.81	−0.19	1.03
P	5.0	5.19	0.19	1.14
La	11.0	9.47	−1.53	1.52

addition of La to FeP_3 increases the depletion around P, an indication of the setup of La bonds.

Results from the Bader analysis in Table 3 show transfer of electrons from the *M* site to the P site. This behaviour is confirmed in previous experimental XPS studies [19,53] and in a recent EELS study [54], where transfer of electrons from Co to P is observed. However, this EELS study shows an increase of electrons at the Fe site for $LaFe_4P_{12}$, a discrepancy most likely related to the use of different electron charge references. In this study the Bader analysis of $LaFe_4P_{12}$ indicates a significant increase of electrons at the P site, a large decrease at the La site, while the decrease of electrons at the Fe site is similar in both FeP_3 and $LaFe_4P_{12}$. The depletion and occupancy numbers both yield results expected from the electronegativity differences. To complement the above analysis we will now consider the spatial distribution of ρ_b.

From the inter-ionic line extraction of ρ_b in Fig. 3 it is clear that there is a significant buildup of electrons between *M* and P. Previous studies have suggested a mainly covalent character of these bonds [9,53]. This is confirmed in this study by the good agreement between the location of the maximum x_b and the centre of electronegativity χ^* from Table 4. Changing *M* yields virtually no change close to the P ions, while there is significant change close to *M*. The influence of the addition of La to FeP_3 is minor for the Fe–P bond as can be seen from Fig. 3.

Table 4
Electron density difference maxima ρ_b^{max} and their normalized relative distance x_b for all significant bond directions for CoP_3, FeP_3 and $LaFe_4P_{12}$. Bond lengths *x* are shown for reference. In addition the centre of Pauling electronegativity χ^* defined in the text is given (Pauling electronegativities for each atom are listed in Table 2).

	x [Å]	ρ_b^{max} [Å^{-3}]	x_b	χ^*
CoP_3				
Co–P	2.22	0.16	0.6	0.54
P–P	2.35	0.19	0.5	0.5
	2.26	0.23	0.5	
FeP_3				
Fe–P	2.22	0.16	0.6	0.55
P–P	2.37	0.17	0.5	0.5
	2.26	0.22	0.5	0.5
$LaFe_4P_{12}$				
Fe–P	2.25	0.14	0.59	0.55
P–P	2.38	0.14	0.5	0.5
	2.30	0.20	0.5	0.5
Fe–La	3.39	0.17	0.09	0.38
	3.39	0.03	0.36	0.38
	3.39	0.02	0.74	0.38
P–La	3.01	0.02	0.72	0.33

The P–P bonds in Fig. 4 are covalent with two different bond lengths. The maximum value of ρ_b in Table 4 shows that the shortest bond dominates in strength. Furthermore, the P_4 ring changes quite drastically from CoP_3 to $LaFe_4P_{12}$. In CoP_3 the shortest length is facing the filler position, while in $LaFe_4P_{12}$ this is opposite. Also, the rectangular P_4 ring in CoP_3 is transformed into a more square shape in $LaFe_4P_{12}$, in correspondence with Ce filled $CoSb_3$ [55]. The likely explanation for this is that the La atoms bond to the nearby dodecahedra of P ions by redistributing electrons from the short P bond to the bond between P and La. This results in a weaker P–P bond close to the La ion, thus increasing the distance between the P ions. As a consequence there is an interchange of the short and long P–P bonds. In light of the previous discussions of the Fe–P bond it is clear that adding La to FeP_3 yields differences primarily in the P_4 ring.

3.3. Electron transfer analysis around the lanthanum atoms

Addressing the La bonds in $LaFe_4P_{12}$ is more complicated. From Fig. 3 and Table 4 there are signs of an ionic character of the P–La bond as indicated in previous work [9]. The relatively weak P–La bond is confirmed in Table 4, where the maximum value of ρ_b between Fe–P and P–La is smaller by an order of magnitude compared to the *M*-P and P–P bonds. A Fe–La bond is unlikely due to the small change of the Fe–La electron transfer between FeP_3 and $LaFe_4P_{12}$ in Fig. 3.

To further investigate the bonding of La, we give the contour plot of ρ_b in the (200) plane in Fig. 5. This plane contains one La ion and four surrounding P ions. Signs of elongated electron buildup (aligned along the crystal axes) are observed, meaning that La possibly interacts with the closest P–P bonds by establishing shared states with both P ions. As a consequence, the P–La bond is not directional between P and La nor ionic. The large depletion cutoff r_d suggests an extended depletion around La. Nevertheless, the elongated electron buildups are established in this zone.

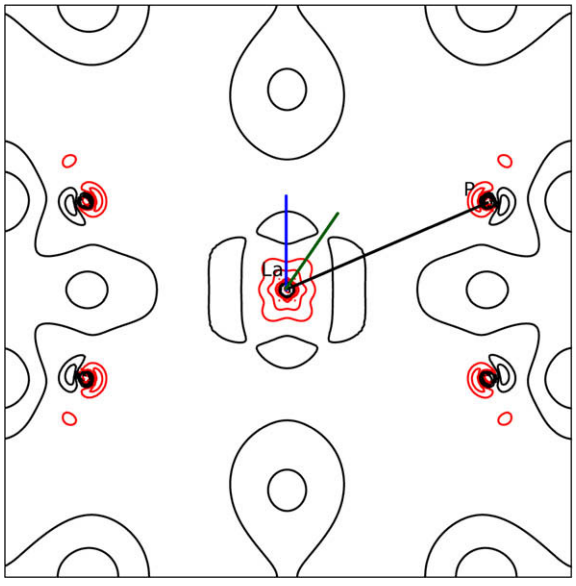

Fig. 5. Contour plot of the electron density difference ρ_b for $LaFe_4P_{12}$ in the (200) plane containing one La surrounded by four P (indicated in Fig. 1). Positive electron transfer (black/dark) are drawn from 0 to 1.0 electrons/Å^3, while the negative (red/light) are drawn from −0.5 to 0 electrons/Å^3, both with a contour spacing of 0.1 electrons/Å^3. The line extraction presented in Fig. 3 is indicated by the solid line. Two different directions are indicated by the blue and green line (see text). (For interpretation of the references to colour in this figure legend, the reader is referred to the web version of this article.)

The elongated electron buildups are likely relevant for the lowering of the lattice thermal conductivity of the filled skutterudites. Vibrations of La along the crystal axes (e. g. blue line Fig. 5) would imply a response from the P dodecahedra and hence be correlated throughout the structure. On the other hand, vibrations along directions between the elongated electron buildup (e. g. green line in Fig. 5 with an additional component normal to the figure plane) are possibly more uncorrelated and anharmonic. Both pictures have been presented in previous studies [10,14,16,15] and we suggest that the peculiar shape of the La–P bonds can explain this apparent contradiction.

4. Conclusions

In this work we investigated the electron transfer in the CoP_3, $LaFe_4P_{12}$ and the hypothetical FeP_3 skutterudite compounds by using the corresponding procrystals as electron charge references.

General agreement with electronegativity considerations was shown. The covalent character of the *M*-P and P–P bonds was confirmed, while a more peculiar character was detected for the P–La bond. It was also shown that the addition of La results in a redistribution of electrons primarily within the P_4 rings.

A unique bonding scheme between P and La was proposed. We showed signs of elongated electron buildup aligned along the crystal axes. Vibrations of the La ion parallel to the crystal axes would be closely connected with the surrounding P_4 rings. In contrast, other vibrational directions would be more uncorrelated throughout the structure. The combination yields a quasi-correlated motion of the La ion, which supports recent [15,16] and previous [10,14] publications, which are apparently contradictory. Studies are in progress to investigate the spatially resolved movement and vibrational properties of the La ion to enlighten this picture.

Acknowledgements

The authors would like to acknowledge support from the Norwegian Research Council and the NOTUR project. In addition we would like to thank Simone Casolo, Ragnhild Sæterli, Ole Bjørn Karlsen and Jon Nilsen for fruitful discussions and ideas.

References

[1] G.J. Snyder, E.S. Toberer, Nat. Mater. 7 (2008) 105–114.
[2] K. Mangersnes, O. Løvvik, Ø. Prytz, New J. Phys. 10 (2008) 053004.
[3] I. Shirotani, T. Uchiumi, K. Ohno, C. Sekine, Y. Nakazawa, K. Kanoda, S. Todo, T. Yagi, Phys. Rev. B 56 (1997) 7866.
[4] G.P. Meisner, Physica B 108 (1981) 763.
[5] D.A. Gajewski, N.R. Dilley, E.D. Bauer, E.F. Freeman, R. Chau, M.B. Maple, D. Mandrus, B.C. Sales, A.H. Lacerda, J. Phys.: Condens. Mat. 10 (1998) 6973.
[6] D.T. Morelli, G.P. Meisner, J. Appl. Phys. 77 (1995) 3777.
[7] M.E. Danebrock, C.B.H. Evers, W. Jeitschko, J. Phys. Chem. Solids 57 (1996) 381.
[8] G.A. Slack, V.G. Tsoukala, J. App. Phys. 76 (1994) 1665.
[9] C. Uher, Semiconduct. Semimet. 69 (2001) 139.
[10] V. Keppens, D. Mandrus, B.C. Sales, B.C. Chakoumakos, M.B. Maple, D.A. Gajewski, E.J. Freeman, S. Bennington, Nature 395 (1998) 876–878.
[11] C. Stiewe, L. Bertini, M. Toprak, M. Christensen, D. Platzek, S. Williams, C. Gatti, E. Müller, B.B. Iversen, M. Muhammed, M. Rowe, J. Appl. Phys. 97 (2005) 044317.
[12] M. Christensen, B.B. Iversen, L. Bertini, C. Gatti, M. Toprak, M. Muhammed, F. Nishibori, J. Appl. Phys. 96 (2004) 3148.
[13] H. Anno, K. Matsubara, Y. Notohara, T. Sakakibara, H. Tashiro, J. App. Phys. 86 (1999).
[14] B.C. Sales, D. Mandrus, B.C. Chakoumakos, V. Keppens, J.R. Thompson, Phys. Rev. B 56 (1997) 15081.
[15] M.M. Koza, M.R. Johnson, R. Viennois, H. Mutka, L. Girard, D. Ravot, Nat. Mat. 7 (2008) 805.
[16] M. Christensen, A.B. Abrahamsen, N.B. Christensen, F. Juranyi, N.H. Andersen, K. Lefmann, J. Andreasson, C.R.H. Bahl, B.B. Iversen, Nat. Mat. 7 (2008) 811.
[17] I. Lefebvre-Devos, M. Lassalle, X. Wallart, J. Olivier-Fourcade, L. Monconduit, J.C. Jumas, Phys. Rev. B 63 (2001) 125110.
[18] M. Llunell, P. Alemany, S. Alvarez, V.P. Zhukov, Phys. Rev. B 53 (1996) 10605.
[19] A.P. Grosvenor, R.G. Cavell, A. Mar, Phys. Rev. B. 74 (2006) 125102.
[20] Ø. Prytz, O.M. Løvvik, J. Taftø, Phys. Rev. B 74 (2006) 245109.

[21] G.S. Nolas, D.T. Morelli, T.M. Tritt, Annu. Rev. Mater. Sci. 29 (1999) 89.
[22] L. Wu, Y. Zhu, T. Vogt, H. Su, J.W. Davenport, J. Taftø, Phys. Rev. B 69 (2004) 064501.
[23] C. Gatti, Z. Kristallogr. 220 (2005) 399.
[24] R.F.W. Bader, Atoms in Molecules: A Quantum Theory, Oxford University Press, New York, 1990.
[25] W. Tang, E. Sanville, G. Henkelman, J. Phys.: Condens. Mat. 21 (2009) 084204.
[26] E. Sanville, S.D. Kenny, R. Smith, G. Henkelman, J. Comp. Chem. 28 (2007) 899.
[27] G. Henkelman, A. Arnaldsson, H. Jónsson, Comp. Mater. Sci. 36 (2006) 254.
[28] Bader analysis code, <http://theory.cm.utexas.edu/bader/>.
[29] R.J. Renka, Trans. Math. Software 14 (1988) 151.
[30] W. Kohn, L.J. Sham, Phys. Rev. 140 (1965) A1133.
[31] P. Hohenberg, W. Kohn, Phys. Rev. 136 (1964) B864.
[36] J.P. Perdew, K. Burke, M. Ernzerhof, Phys. Rev. Lett. 77 (1996) 3865.
[37] P.E. Blöchl, Phys. Rev. B 50 (1994) 17953.
[38] G. Kresse, D. Joubert, Phys. Rev. B 59 (1999) 1758.
[39] G. Kresse, J. Furthmüller, Comp. Mater. Sci. 6 (1996) 15.
[40] G. Kresse, J. Furthmüller, Phys. Rev. B 54 (1996) 11169.
[41] G. Kresse, J. Hafner, Phys. Rev. B 49 (1994) 14251.
[42] G. Kresse, J. Hafner, Phys. Rev. B 48 (1993) 131158.
[43] VASP code, <http://cms.mpi.univie.ac.at/vasp>.
[44] P. Pulay, Chem. Phys. Lett. 73 (1980) 393.
[45] A.D. Vita, PhD Thesis, Keele University, 1992.
[46] M. Methfessel, A.T. Paxton, Phys. Rev. B 40 (1989) 3616.
[47] T. Schmidt, G. Kliche, H.D. Lutz, Acta Crystallogr., Sec. C: Cryst. Struct. Commun. 43 (1987) 1678.
[48] W. Jeitschko, D.J. Braun, Acta Crystallogr. B 33 (1977) 3401.
[49] W. Jeitschko, A.J. Foecker, D. Paschke, M.V. Dewalsky, C.B.H. Evers, B. Kuennen, A. Lang, G. Kotzyba, U.C. Rodenwald, M.H. Moeller, Z. Anorg. Allg. Chem. 626 (2000) 1112.
[50] A.L. Allred, J. Inorg. Nucl. Chem. 17 (1961) 215.
[51] L. Pauling, The Nature of the Chemical Bond, third ed., Cornell University, USA, 1960.
[52] B. Cordero, V. Gómez, M.R.A.E. Plataro-Prats, Echeverria, E. Cremades, F. Barragán, S. Alvarez, Dalton Trans. (2008) 2832.
[53] S. Diplas, Ø. Prytz, O.B. Karlsen, J.F. Watts, J. Taftø, J. Phys.: Condens. Mat. 19 (2007) 246216.
[54] Ø. Prytz, J. Taftø, C.C. Ahn, B. Fultz, Phys. Rev. B 75 (2007) 125109.
[55] H. Kitagawa, M. Hasaka, T. Morimura, H. Nakashima, S. Kondo, Mater. Res. Bull. 35 (2000) 185.